REAL TIME THERMAL IMAGING OF HIGH TEMPERATURE SEMICONDUCTOR MELTS

Michael J. Wargo

Massachusetts Institute of Technology

Cambridge, MA 02139

ABSTRACT

A real time thermal imaging system with temperature resolution better than +/− 1 degree centigrade and spatial resolution of better than 0.5 mm has been developed. It has been applied to the analysis of melt surface thermal field distributions in both Czochralski and liquid encapsulated Czochralski (LEC) growth configurations. The melt is viewed in near normal incidence by a high resolution (512x512) charge coupled device (CCD) camera to which is attached a very narrow bandpass filter (1 nm width centered on 632 nm). The resulting image is digitized (8 bit/pixel) and processed using a pipelined pixel processor operating at an effective 40 million operations per second thus permitting real time high frequency spatial and temporal filtering of the high temperature scene. The dual ported nature of the digital storage units allows the parallel processing of the optical intensity data by off−loading the task to the main CPU, floating point accelerator and array processor. In this way, graphics overlays are generated which display concurrently processed data with no performance penalty on image processing.

A multi−pixel averaging algorithm has been developed which permits localized, low noise sensing of temperature variations at any location in the hot zone as a function of time. This signal is being used to implement initial elements of a feedforward growth control scheme which is aimed at reducing thermal disturbances to the melt caused by the batch nature of the growth process. The effect of magnetic melt stabilization (with axial fields of up to 5 kgauss) on radial melt temperature distributions has been measured using this technique. Presently, the system is capable of measuring only relative temperature differences. Problems associated with residual internal reflections and non−optimized optical path geometry are discussed.

Introduction and Background

The growth of semiconductor single crystals by the Czochralski crystal pulling technique and, in particular, the growth of compound semiconductors like GaAs using the liquid encapsulated Czochralski (LEC) technique, requires precise control of the thermal field within the melt and growing crystal. The spatial temperature distribution in the melt is established by the hot zone, crystal and environmental thermal boundary conditions. In conventional growth systems, a single−input−single−output (SISO) closed loop proportional, integral and derivative (PID) controller is used to maintain and/or change a single temperature to accomplish the task of controlling the temperature distribution in the melt. Thermocouples or single color pyromters are generally used as the sensors for this purpose. As shown in figure 1, the location of the single point temperature sensor is typically well

Conventional Control Points

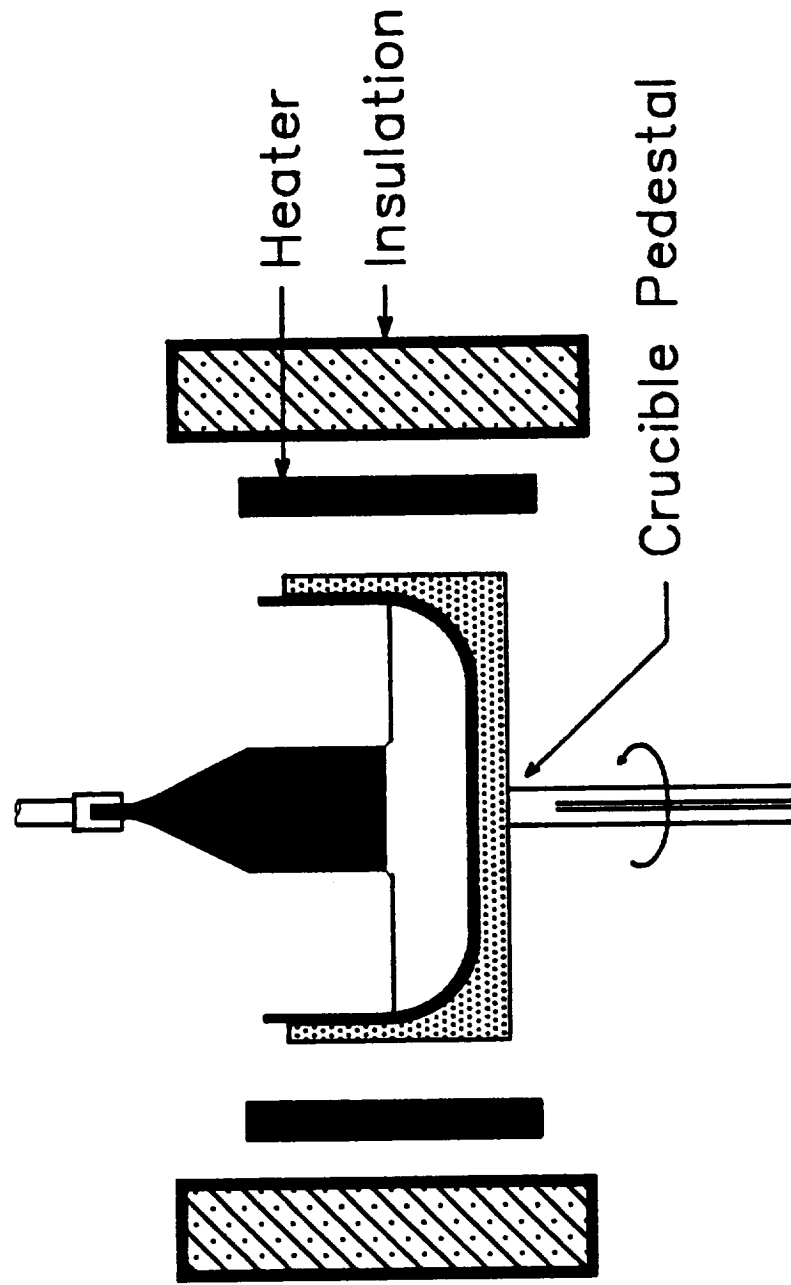

Heater

Insulation

Crucible Pedestal

Figure 1 Locations of temperature sensors for control in conventional Czochralski and Liquid Encapsulated Czochralski (LEC) growth configurations. Typical sensors include thermocouples and optical pyrometers.

removed from the area of measurement interest: the melt/crystal interface. The sensor's placement is determined empirically. Passive means are also used to influence the temperature distribution in the melt and growing crystal. These include choice of the axial position of the crucible within the hot zone and heat shields to modify the heat transfer to and from the crystal/melt system.

The non-axisymmetric nature of the melt surface temperature distribution is known to cause periodic fluctuations in the microscopic rate of growth during rotational pulling [1]. The commensurate variation in electronic materials properties (e.g. carrier concentration) contributes to the inability of solid state semiconductor matrices to perform near their theoretical limits. Turbulent convection is present in large Czochralski melts due to unavoidable radial and axial temperature gradients. The effects of the random melt temperature fluctuations associated with turbulence are exhibited in the grown crystal as chaotic variations in dopant concentration superimposed on the periodic rotational variations discussed above. Application of a magnetic field to the melt has been shown to eliminate melt turbulence and its related effects on growth and segregation [2]. However, the application of the field has also been observed to change the magnitude of the radial temperature gradient [3]. Since the radial temperature gradient controls to a major extent the sensitivity of the crystal diameter to overall changes in hot zone temperature, the quantitative evaluation of the melt surface thermal field is critical to the development of an improved control scheme for the crystal growth process. To this end, a real time thermal imaging system has been developed. In addition, the imager has been used as an advanced sensor to control the temperature of the hot zone from positions nearer the critical phase transformation boundary.

Theoretical Basis for Image Interpretation

Wien's approximation [eq. 1] to Planck's radiation law is used to establish a relationship between changes in optical intensity (I), temperature (T) and wavelength (λ).

$$I(\lambda,T) = C_1 \epsilon(\lambda,T)/\lambda^5 \, [\exp(-C_2/\lambda T)] \qquad [1]$$

C_1 and C_2 are constants, 3.7403×10^{-4} watt μm^2 and 1.438×10^4 $\mu m^\circ K$ respectively and ϵ is the emmisivity of the melt. In the first development phase, experiments were conducted to determine a direct relationship between intensity and temperature. (The thermal imager was calibrated using two methods. See section on temperature control by thermal imaging.) Work is presently in progress to quantitatively determine the input/output characteristics of the CCD camera used for the image acquisition. (See next section.) Once this is accomplished, the optical path will then be included in the calibration scheme so that the absolute intensity will be measured during an experiment. In this way, a direct, quantifiable relationship will exist between the measured intensity and the absolute temperature.

Hardware Configuration and System Architecture

The operation of the thermal imager is based on the same theoretical principles as single color optical pyrometry. The high termperature scene (the encapsulated GaAs melt) is viewed in near normal incidence by a high resolution (512 x 512 pixels) low noise (-60 dB) charge coupled device (CCD) camera (RCA). In this way, an array of 1/4 million discrete optical pyrometers are available to characterize the scene with a spatial resolution of better than 0.5 mm. A very narrow band pass filter (1 nm width, centered at 633 nm) is placed between the scene and the camera to obtain a monochromatic image. The transmission wavelength of the filter was chosen to match the peak in the spectral sensitivity of the CCD element while maintaining a steep slope on the I vs T curve of the emitting surface (the melt).

A schematic of the thermal imaging architecture and a preliminary control structure is shown in figure 2. The major components include the growth system (modified Hamco CG-800) with axial superconducting magnet (5 Kgauss, American Magnetics), the CCD camera and narrow bandpass filter, the image processing subsystems (Recognition Technology, Inc.) with high resolution analog RGB monitor and the host computer with integral high speed data acquisition and control capability (Masscomp MC-5500).

The camera generates information at 30 frames/second using a standard RS-170 configuration. Adjustment of gain and dc offset of the CCD camera's analog output is accomplished in the analog to digital subsystem. This permits operation at high gain for maximum sensitivity. At this time, the signal is pre-processed with user defineable look up tables (LUT) to correct for inherent non-linearities within the camera and digitized to 8 bits (256 gray levels). Image processing functions are carried out in the pipelined pixel processor. (For an in-depth description, see next section.) Other principle tasks include image storage and transfer within the digital storage units. A unique capability of the system is the dual ported nature of the digital storage units. Image memory appears as extended system memory on the host. As a result, image data can be accessed simultaneously by the pipelined pixel processor and the host CPU. In this way, parallel processing of the information can be accomplished with no performance penalty. Real time graphics overlays and linear convolutions are produced in this manner. Two of the digital storage units are configured as a 16 bit pair to hold high precision intermediate results produced during certain image processing calculations (e.g. 2-d convolutions and temporal averaging, see next section). A third 1024 x 1024 image memory unit is configured as four contiguous 512 x 512 frame stores.

The processed images (in real time) are sent back through the A/D subsystem where a second LUT is used to false color the outgoing monochrome signal. The LUT is defined to map low intensities to blue and high intensities to red with a linear interpolation of the complete 8 bit dynamic range. In

387

Thermal Imaging Architecture With
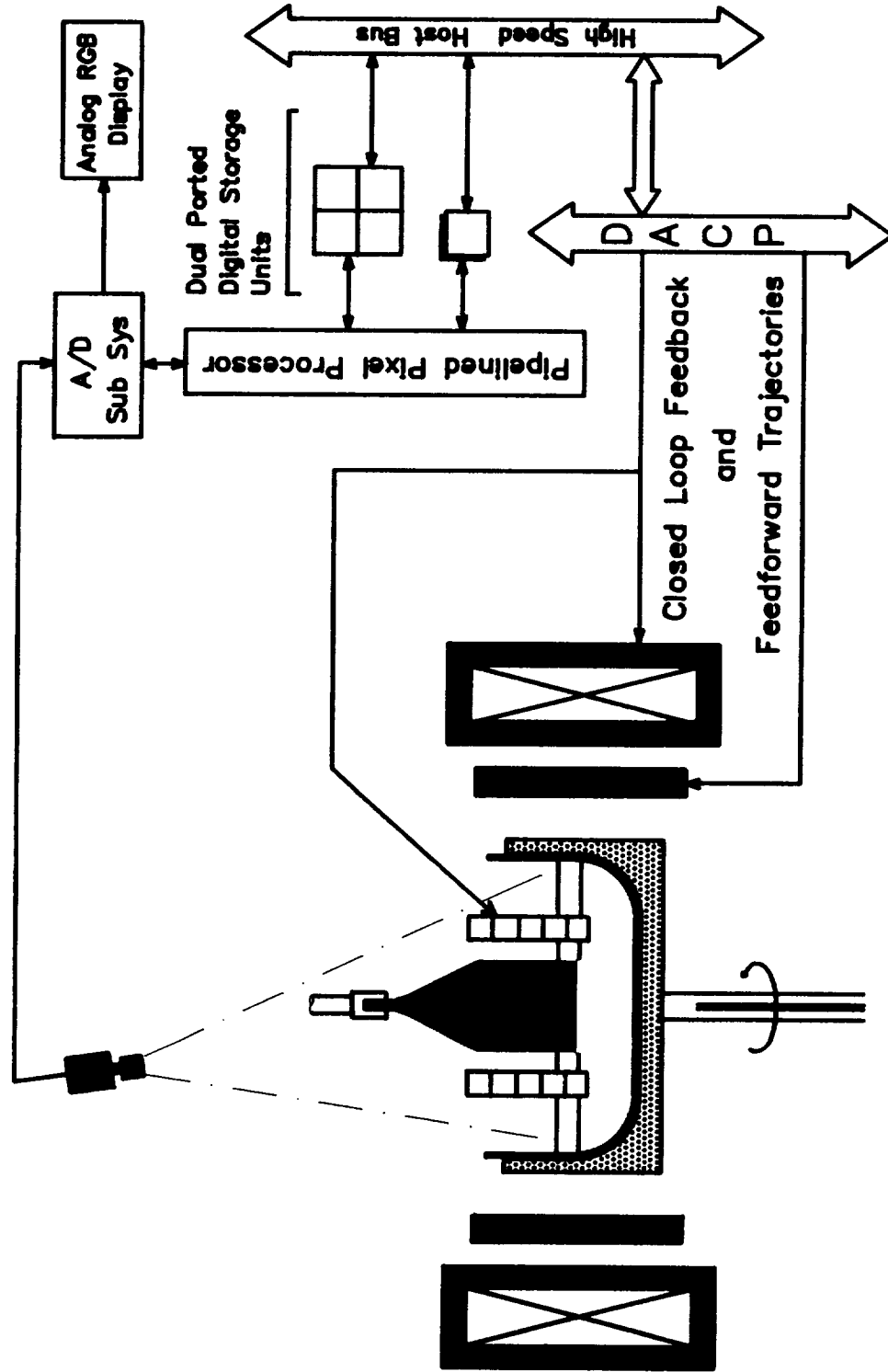# Preliminary Control Structure

Figure 2

Thermal imaging architecture and preliminary control structure for LEC growth of GaAs. The use of closed loop feedback and feedforward trajectories are discussed in detail in reference 4. Non-traditional control elements include the heat exchange system (HES) around the growing crystal and the superconducting magnet around the furnace.

388

this way, a complete spectrum between blue and red corresponds to intensities from 0 to 255 gray levels. The output is displayed (with graphics overlays) on a high resolution RGB monitor.

Thermal information is selectively extracted from the thermal image and passed, via the host, to the Data Acquisition and Control Processor (DACP). In this mode, the raw thermal data is scaled and offset to conform to the required output characteristics (e.g. a platinum/platinum10% rhodium thermocouple) and sent from a digital to analog (D/A) converter to the crystal puller to be used for temperature control. Figure 2 also indicates alternate strategies for systems control from the thermal imager. Development is currently in progress to adjust, by computer, the magnitude of the axial magnetic field for closed loop control of the radial temperature gradient in the melt based on a line scan of the surface temperature field obtained from the thermal imager. In like manner, the thermal field within the growing crystal will be controlled through a heat exchange system (HES) mounted coaxially about the growing crystal.

Thermal Imaging of High Temperature Semiconductor Melts

The thermal imaging geometry is illustrated in figure 3. The CCD camera is, by necessity, mounted off-axis and non-normal to the melt surface. The crystal pull shaft is on the rotational axis and the camera axis is located 3.5 inches from it inclined at 5° to the normal. As a result, internal reflections from the melt surface are reduced but not totally eliminated. The high temperature scene comprises the melt, crucible, heater elements, crystal and pull shaft. However, the only portion of the scene which provides optical information that is readily convertible to temperature is that which is emitted from the surface of the melt.

A raw (unprocessed, single frame) thermal image of a conventional LEC GaAs melt just prior to seeding is shown in figure 4. False color representation of the high temperature scene depicts high melt temperatures as red and lower temperatures as progressively bluer. The horizontal line crossing the encapsulated melt represents a linear array of picture elements (pixels) from which temperature data is extracted, processed and displayed in real time. This data is shown in the curved line above the displayed horizontal pixel array. It has been processed by a linear convolution to remove high spatial components. This processing was offloaded from the pipelined pixel processor to the main CPU to maintain real time performance. The gray level scale on the ordinate corresponds directly to temperature. (Calibration of the gray scale is discussed below.) Thus, the slope of the line indicates the magnitude of the radial temperature gradient. Shown in the image are the bubbles inevitably present just following the melting of the charge. It is clear that the bubbles mask any temperature information in that region of the image. However, continuous temporal averaging of consecutive images (with exponential de-emphasis of previous frames) can be used to 'eliminate' the effect of
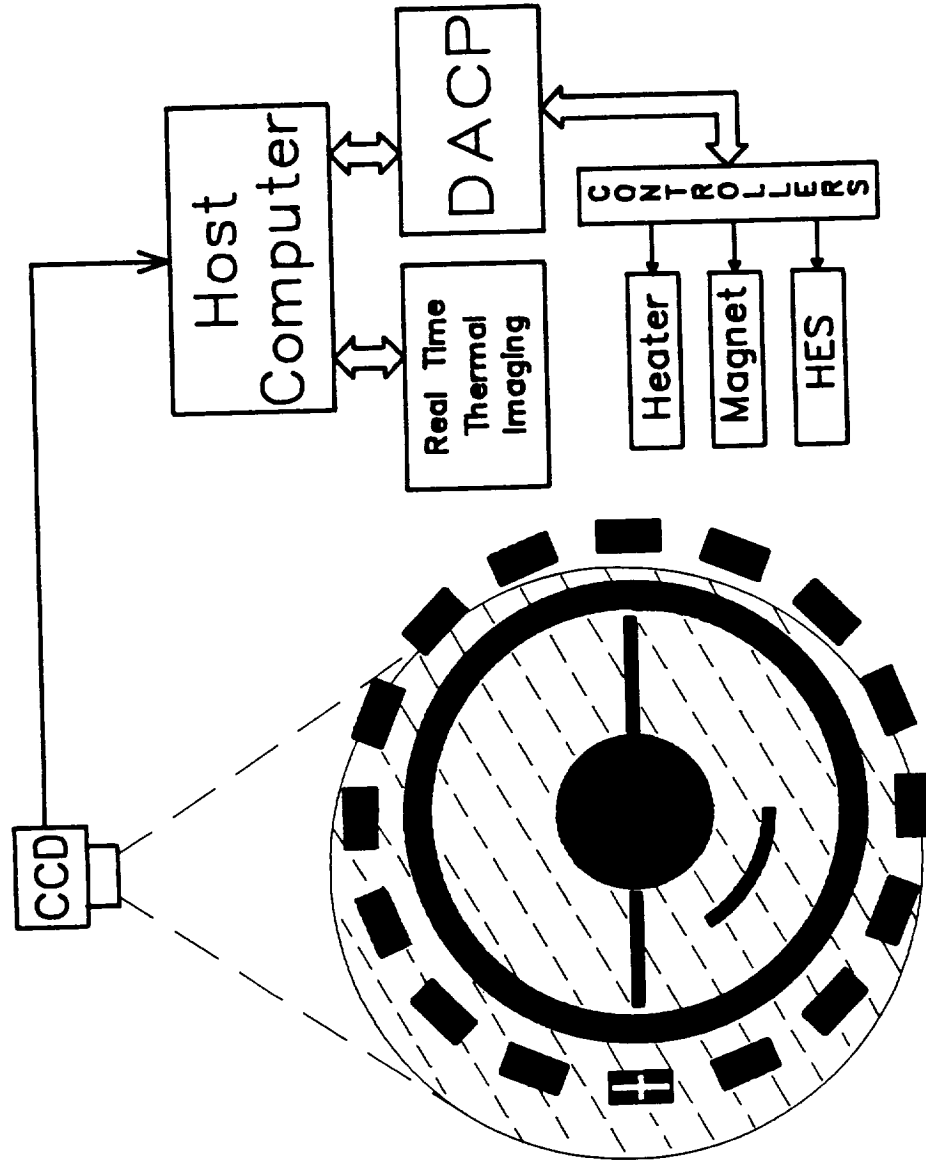
.

Figure 3

Geometry of thermal imaging system. Alternative temperature sensing locations and geometries are indicated. At present the line scan across the melt and crystal and the single point (cross-hair at heater element) have been implemented. Only the single point approach is currently used for control.

these spatial perturbations (figure 5). The temporal averaging facility operates in real time and the number of frames averaged is user selectable.

Figure 6 is a thermal image taken during the initial stages of GaAs growth. The bright disk just below the seed shaft is the growing crystal. It appears bright (red, in false color) due to the higher emissivity of the solid compared to the melt as well as its reflecting the high temperature information coming from the crucible wall. The intensity does not, in this case, unambiguously reflect the temperature of the crystal. With more quantitative information about the emissive nature of the crucible and crystal this temperature distribution could also be determined. Even so, the abrupt discontinuity of the optical intensity observed on crossing the melt/crystal boundary provides useful information concerning the diameter of the growing crystal and can, in principle, be used as a feedback signal for diameter control. This measurement has significant advantages compared to the differential weight which is used in conventional LEC growh systems for ADC (automatic diameter control) [4].

Figure 7 shows the same growth conditions but with the application of a 2000 gauss axial magnetic field. Comparison of the displayed data with figure 6 (no field) indicates the increase in radial temperature gradient caused by the magnetic field. The magnetic field reduces the convective component of heat transfer in the melt. Since the heat lost from the crystal is not influenced by the magnetic field, the temperature distribution in the crystal is not expected to be modified. Thus, an increased radial temperature gradient in the melt is required to bring, by conduction alone, the same amount of heat to the crystal/melt interface. Based on a measured gray level to temperature correspondence of $0.5°C$/gray level (see section on systems calibration), the radial temperature gradient in the absence of the field was less than $5°C$/cm whereas the temperature gradient with melt stabilization of 2000 gauss was in excess of $10°C$/cm.

High spatial frequency noise in a thermal image can be eliminated on a full frame basis. Such a two dimensional convolution is performed in n frame times where n is the the number of non−zero elements in the convolution kernal (typically 8 of 9 in a 3 x 3 matrix). Thus, a complete convolution is accomplished in 8 frame times or 8/30 second. This technique is illustrated in figures 8 and 9. Figure 8 is a single frame thermal image. Isotherms, corresponding to constant intensity contours, are revealed by highlighting selected gray levels. Note the diffuse nature of the isotherm representation. In figure 9, the convolved image illustrates a reduction in high spatial frequency noise. Isotherms are now depicted in a more coherent form.

The foregoing thermal imaging capabilities are characterized by a view of the scene and display of the data at a single point in time (though it may have been time averaged). Another approach, found to be useful for systems control purposes, is to acquire and display intensity (temperature) data as a continuous function of time. Figure 10 shows the result of a pixel averaging alogorithm

which takes intensity data from an n x m array of pixels (in this case, 3 x 3), arithmetically averages it and displays the results in real time overlayed on the thermal image.

System Calibration

Two techniques were employed to calibrate the thermal imager. Both permit relative but not absolute determination of the temperature; i.e. only temperature changes are measureable quantitatively. In the first approach, a magnetically stabilized melt was imaged at three different temperatures separated by 10°C (figure 11). (These temperature changes were accomplished using a conventional temperature control scheme where the sensing thermocouple is in close proximity to the heater.) In each image, the same three isotherms, 20 gray levels apart, are highlighted. At temperature, T, all three isotherms are visible; it is hottest at the crucible wall, coldest at the center of the melt. At T+10°C, the innermost (coldest) isotherm has all but disappeared and its previous position (at T) has been taken by the second (middle) isotherm. This near replacement of isotherms is repeated once more at T+20°C. Now the third isotherm (originally near the crucible wall) is in approximately the same position as that of the first isotherm at temperature, T. This indicates that, over this temperature range, approximately 20 gray levels correspond to 10°C. Or, the sensitivity of the thermal imager is given as 0.5°C per gray level. The second calibration was conducted without a melt in the crucible but with a thermocouple present to directly measure temperature changes at one location. Using the algorithm described above for measuring the optical intensity at a point, the output of the thermal imager was amplified, scaled, processed by a digital to analog converter and directly compared to the response of the thermocouple. The pixel array chosen was 9x9. The results (figure 12) show that there is a direct relationship between the changes measured by the thermocouple and the signal produced by the thermal imager. While the output of the thermal imager is represented in the figure in volts, it corresponds to the same value for calibration of the system as the first method: 20 gray levels for every 10°C.

Temperature Control by Thermal Imaging

As previously indicated, conventional temperature control schemes in LEC growth configuration (figure 1) are based on sensor locations which are well removed from the critical area of interest. Using the thermal imager as an advanced single point temperature sensor, it was possible to control the temperature of the growth system from a more advantageous position within the crucible. The intensity (temperature) information from the imager was re-scaled (gain and d.c. offset) so that the output of the D/A converter, after processing by a 1000:1 voltage divider, corresponded directly to that of a Pt/Pt–10%Rh thermocouple. In this way, the signal could be fed to the conventional, analog PID controller which had previously been used to control a thermocouple placed near a heater ele-

ment. Figure 13 shows the results of 5°C control changes made with the analog controller. The output of the thermocouple located within the crucible and the old control thermocouple (at the heater) were recorded. In both cases, the change in output corresponds to the temperature changes made at the controller indicating that the signal from the thermal imager successfully tracked and measured the temperature response of the system. The ringing (decaying, oscillatory) component of the temperature response recorded by the thermocouples reflects the non−optimized PID parameters of the analog controller. These values were left unchanged from those previously determined for the thermocouple sensing the heater temperature. Considerably improved control performance would be achieved with the retuning of the PID settings.

Discussion

Three fundamental assumptions are made which permit, in LEC growth configuration, the interpretation of the output of the thermal imager as temperature information. First, to eliminate any effect of internal reflections, the high temperature scene is viewed in normal incidence. Second, the emissivity of the melt does not change over the temperature range of interest. And, third, the characteristics of the optical path are time independent. It is important to recognize how closely these assumptions are adhered to in the present experimental configuration as well as what effect any deviation from them has on the interpretation of the images. Finally, approaches to reducing or eliminating these effects are considered.

As indicated in figure 2, the camera is mounted inclined about 5° to the normal. The effect of this deviation from normal incidence is most evident during observation of melts. Isotherms appear to be shifted from a centro−symmetric position. However, when an empty graphite crucible (with roughened surface) is imaged, no effect of the non−normal incidence is observed; isotherms are concentric about the center of the crucible. This indicates that high temperature information from the crucible walls is being reflected from the melt surface to the thermal imager. Work is currently in progress to negate this effect with a correction technique that subtracts from the live image a reference image containing information characteristic of the reflection.

There is currently no indication that the emissivity of the melt changes significantly over the temperature range encountered during a typical growth emperiment. However, an effective change does occur if, for example, the perturbations associated with bubbles are considered. In this case, the temporal averaging algorithms are being modified to be included in the systems control module of the computer code. This will eliminate the radical transients measured by the imager as a result of bubbles crossing control point.

One significant change that does occur over the course of a growth run is the characteristics of the optical path. During this time: 1. The window through which the imager views the melt gradu-

ally becomes covered with material which has condensed from volatile melt constituents that are not totally contained by the liquid encapsulant. 2. The optical transparency of the encapsulant changes as its chemistry is modified by the disolution of melt and dopant components. Two approaches to this problem are being pursued. In a manner similar to that discussed above to deal with the internal reflection problem, image subtraction can correct for changes in the optical path as long as these changes are reproducible and well characterized. It is preferable, however, to eliminate both the clouding effect as well as the window coating by development of alternative encapsulants which do not suffer from the limitations encountered with the use of the conventional encapsulant, boric oxide. Work is in progress in this area.

Summary

A high resolution thermal imaging system which operates in real time has been developed. It has been used to characterize the radial temperature distributions in high temperature semiconductor melts. This system also operates as an advanced non-contact temperature sensor and has been used to actively control the temperature of a low pressure LEC GaAs crystal puller. High performance spatial and temporal filtering algorithms have been applied to reduce high spatial frequency noise inherent in both the process and the measurement. This technique is potentially well suited to thermal characterization and control of other materials processing technologies. The non-contact aspect of the design makes it attractive to those applications where non-invasive measurement of temperature is required.

Acknowledgements

References

1.   K. Morizane, A.F. Witt and H.C. Gatos, J. Electrochem. Soc. 114 (7) 738 (1967).
      A.F. Witt and H.C. Gatos, J. Electrochem. Soc. 115 (1) 70 (1968).

2.   A.F. Witt, C.J. Herman and H.C. Gatos, J. Materials Science 5 822 (1970).
      K. Hoshikawa , Jap. J. Appl. Phys. 21 (9) L545 (1982).
      K. Hoshikawa, H. Kohda and H. Hirata, Jap. J. Appl. Phys. 23 (1) L37 (1984).

3. M. J. Wargo and A. F. in preparation for J. Crystal Growth.

4. M. A. Gevelber, M. J. Wargo and G. Stephanopoulos, accepted for publication in J. Crystal Growth.
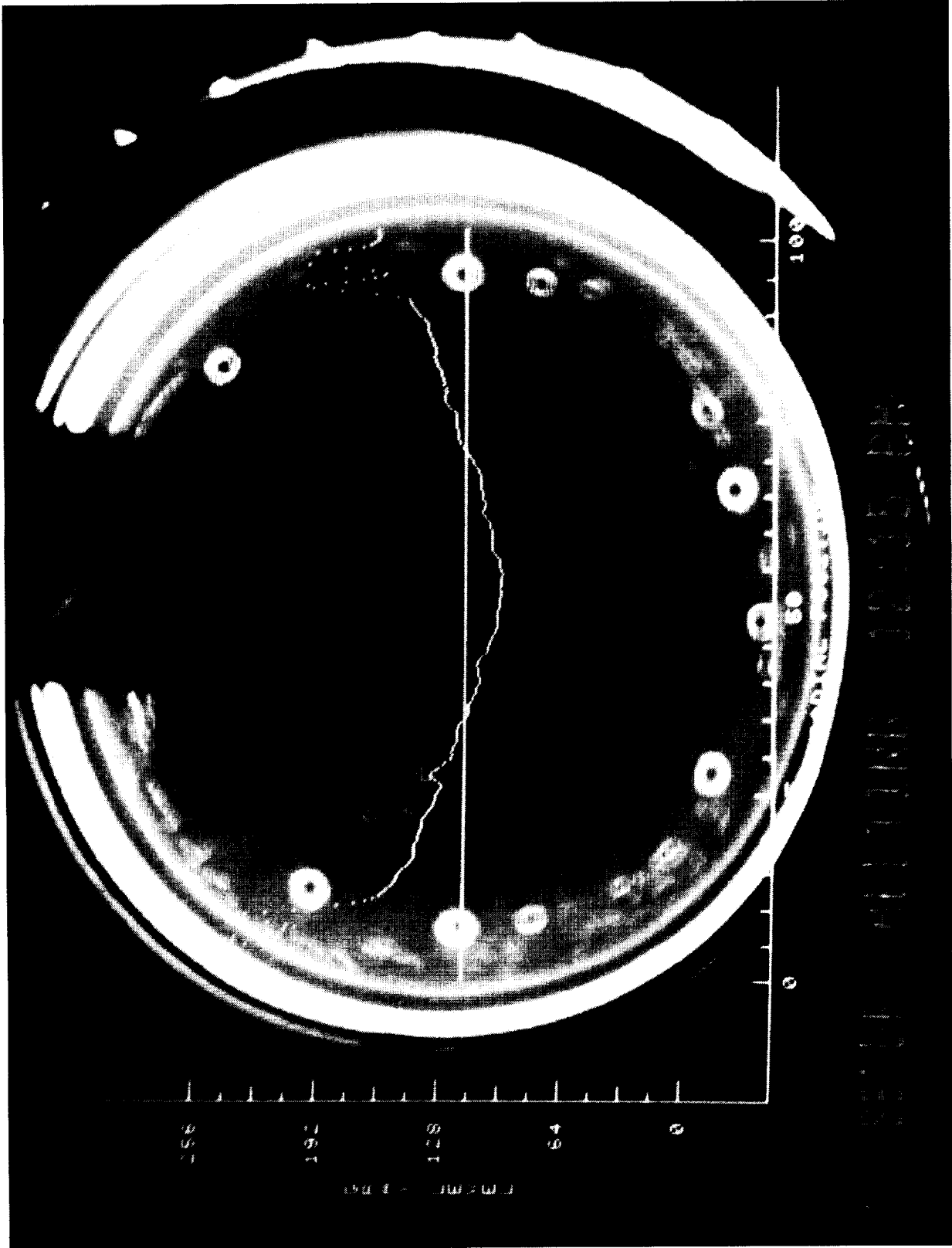
Figure 4   Thermal image of an encapsulated GaAs melt. No processing has been done on the image. However, the data plotted in the graphic overlay has been subjected to a linear convolution to remove high spatial frequency noise.
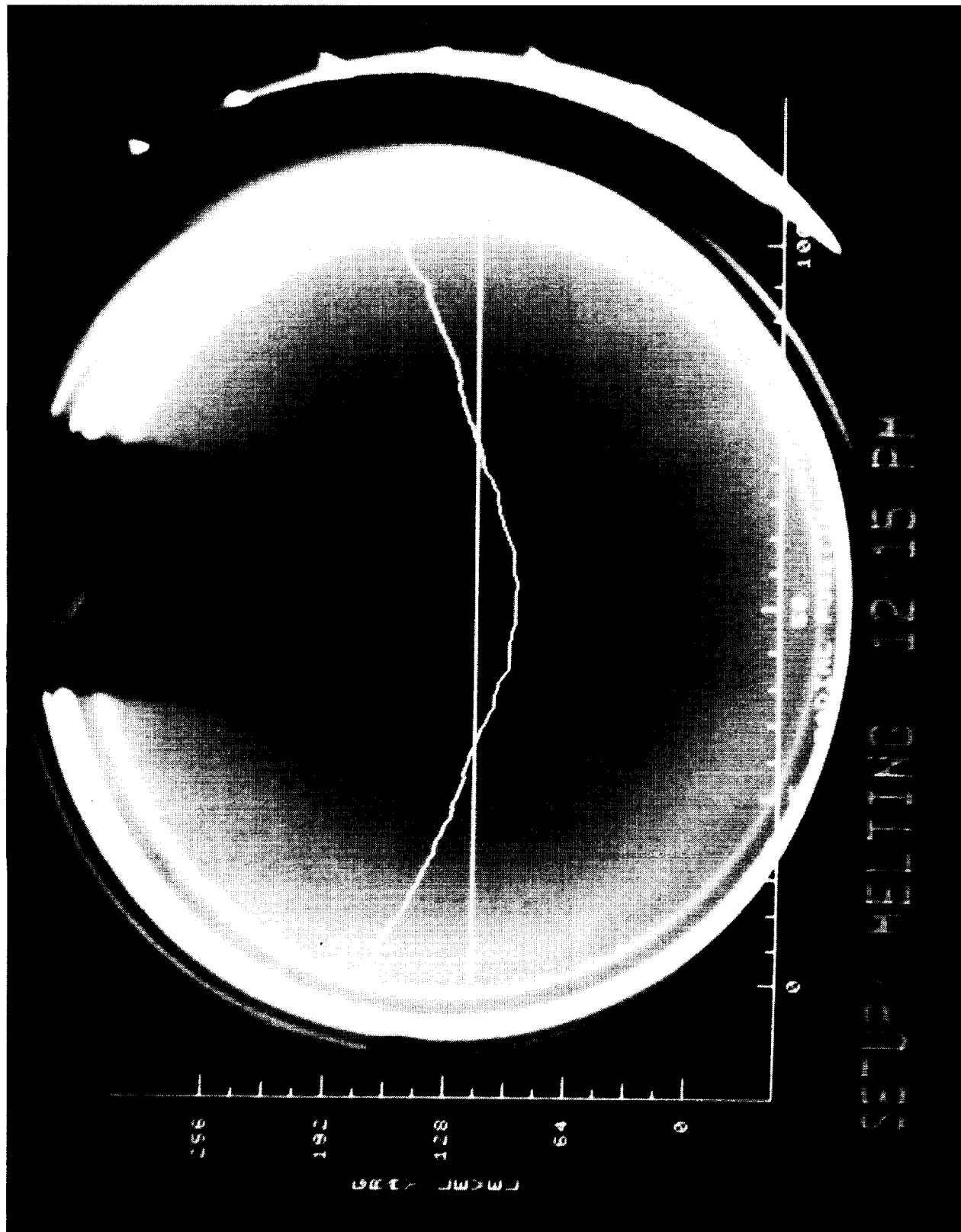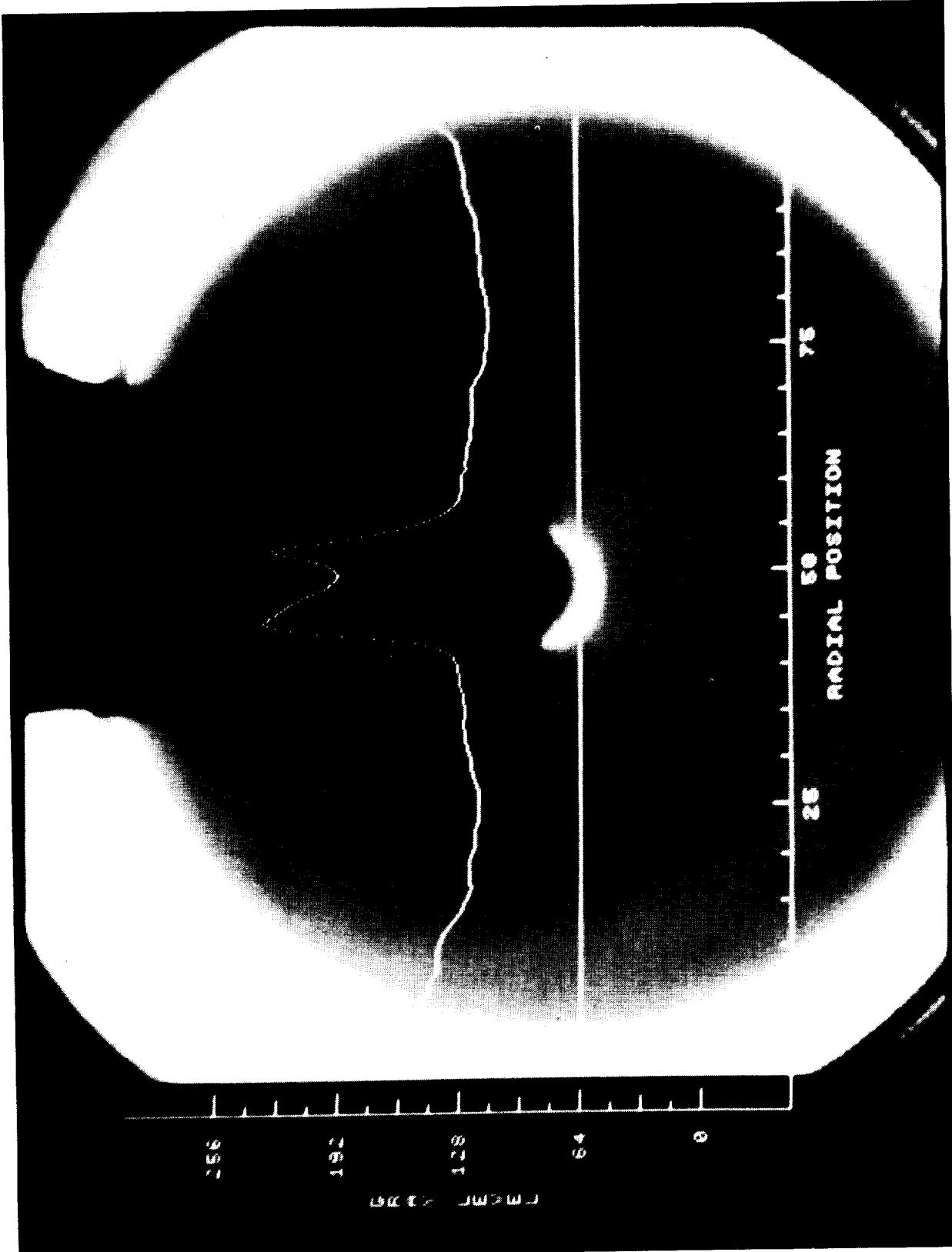
Figure 5   Thermal image of an encapsulated GaAs melt. Temporal averaging has been used to 'eliminate' the effect of the bubbles.

397

Thermal image of an encapsulated GaAs melt taken during the seeding process. No magnetic field is applied. Note the low radial temperature gradient indicated by the limited gray scale range of the intensity distribution across the melt.
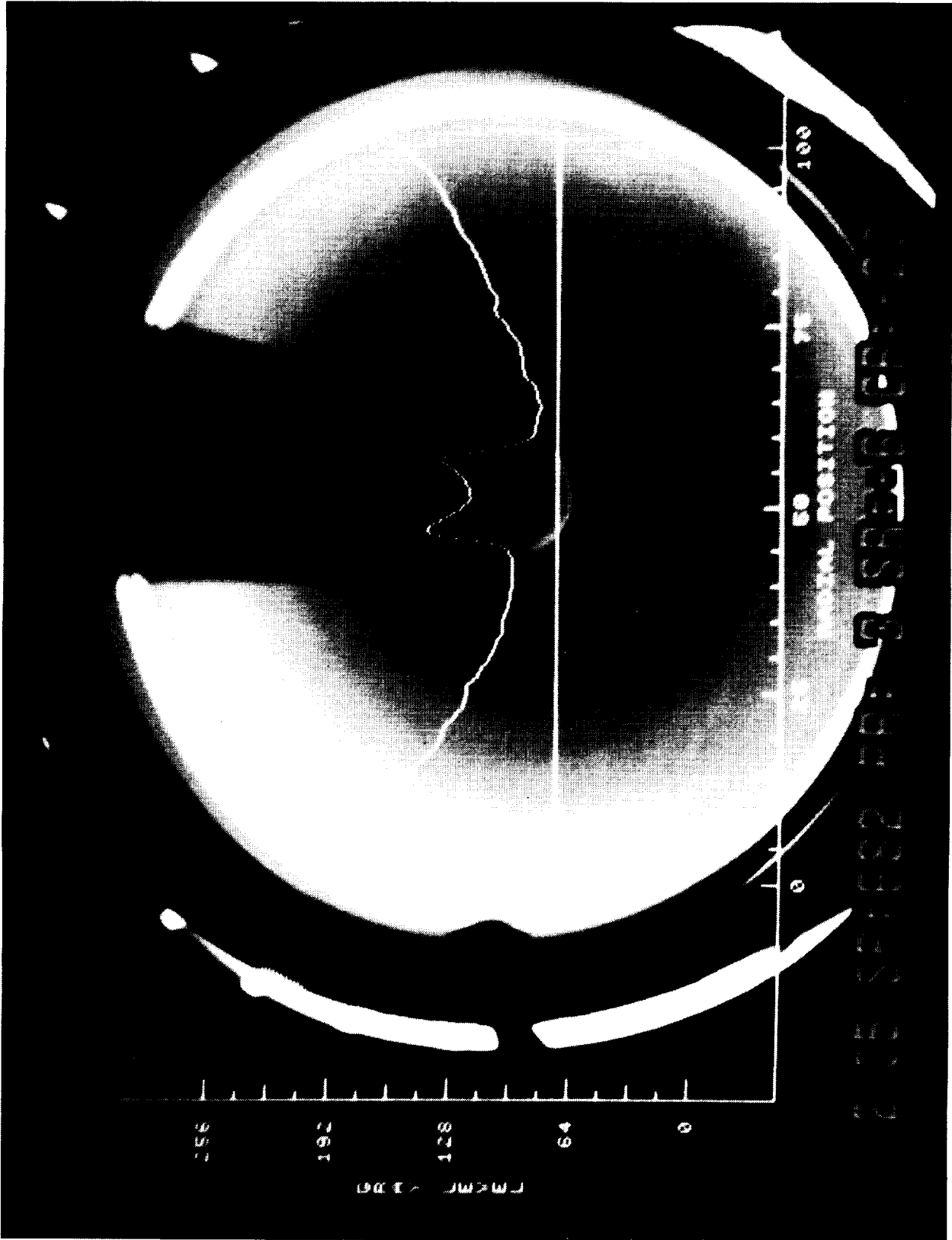
Figure 6

Thermal image of an encapsulated GaAs melt with an applied magnetic field of 2000 gauss. All growth conditions are the same as figure 6 except for the presence of the field. The radial temperature gradient is substantially increased.
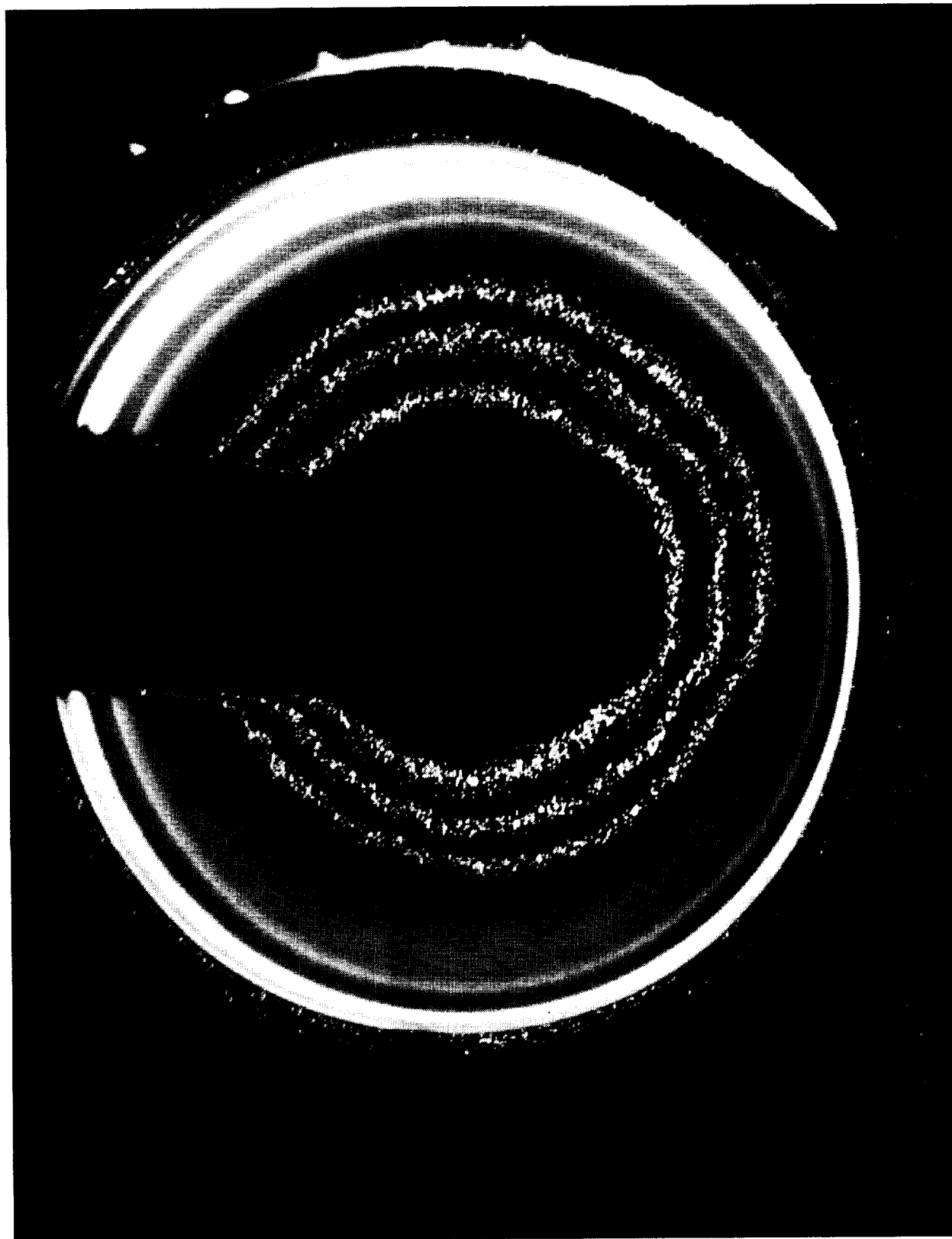
Figure 7

Figure 8 _Isotherm representation on an encapsulated GaAs melt: 3000 gauss. No image processing has been applied to reduce high frequency spatial noise. Note the spatially diffuse nature of the isotherms.

400

Figure 9   Isotherm representation after application of a two dimensional low pass filtering convolution utilizing a 3 x 3 convolution kernal. Note the reduction in high spatial frequency noise resulting in a more coherent representation of the isotherms.

401
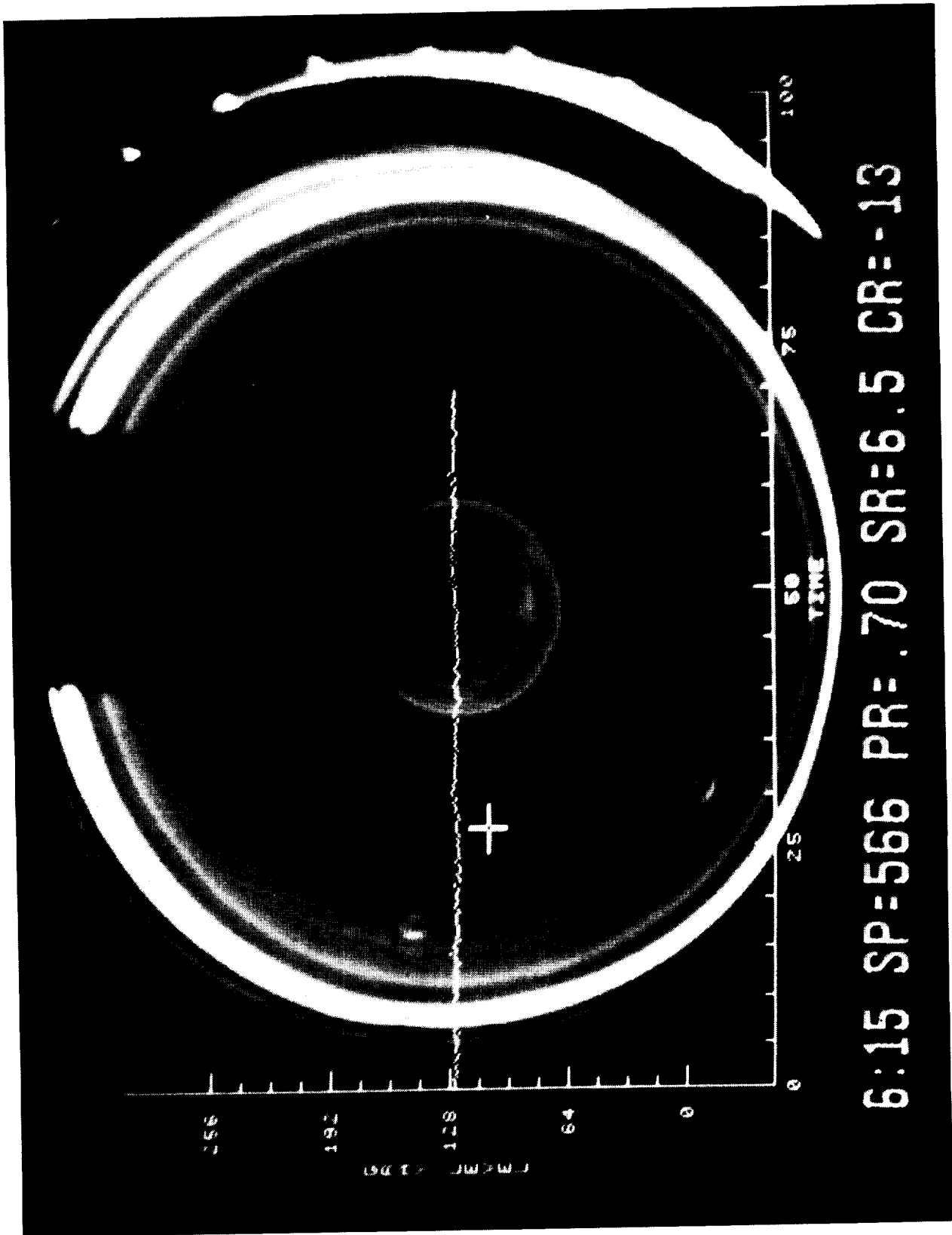
Figure 10 Thermal image of an encapsulated GaAs melt with graphic display of the output of a multi-pixel averaging algorithm. The optical intensity (temperature) data is taken from a single point (defined by the cross–hair) and displayed in real time.
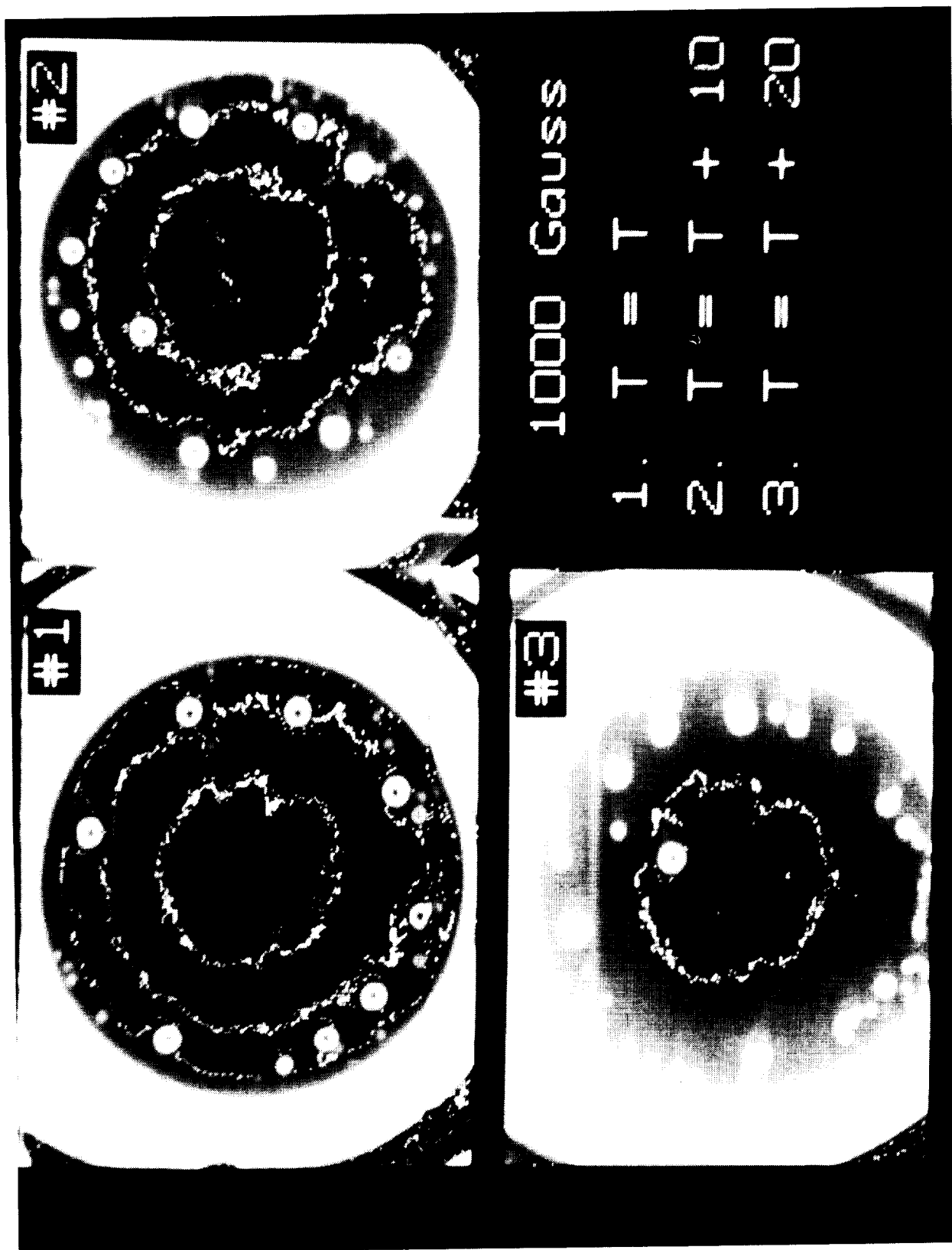
Figure 11 Calibration of the thermal imager. Three thermal images are depicted where the temperature increases in 10°C increments between them. The isotherms shown in each image are at the same gray levels. See text.

Temperature (PID) Control by Thermal Imager (9X9 pixel avg)

Figure 13

Temperature control of an LEC GaAs puller using the thermal imager as an advanced sensor. Temperature changes are 5°C. The plot on the left is the output of a thermocouple located in the crucible. The plot on the right is the output of the thermocouple used for conventional control located at the heater (Note change in scale). The ringing in the control response is due to non-optimized PID parameters used with the conventional controller which was driven by the imager. See text.
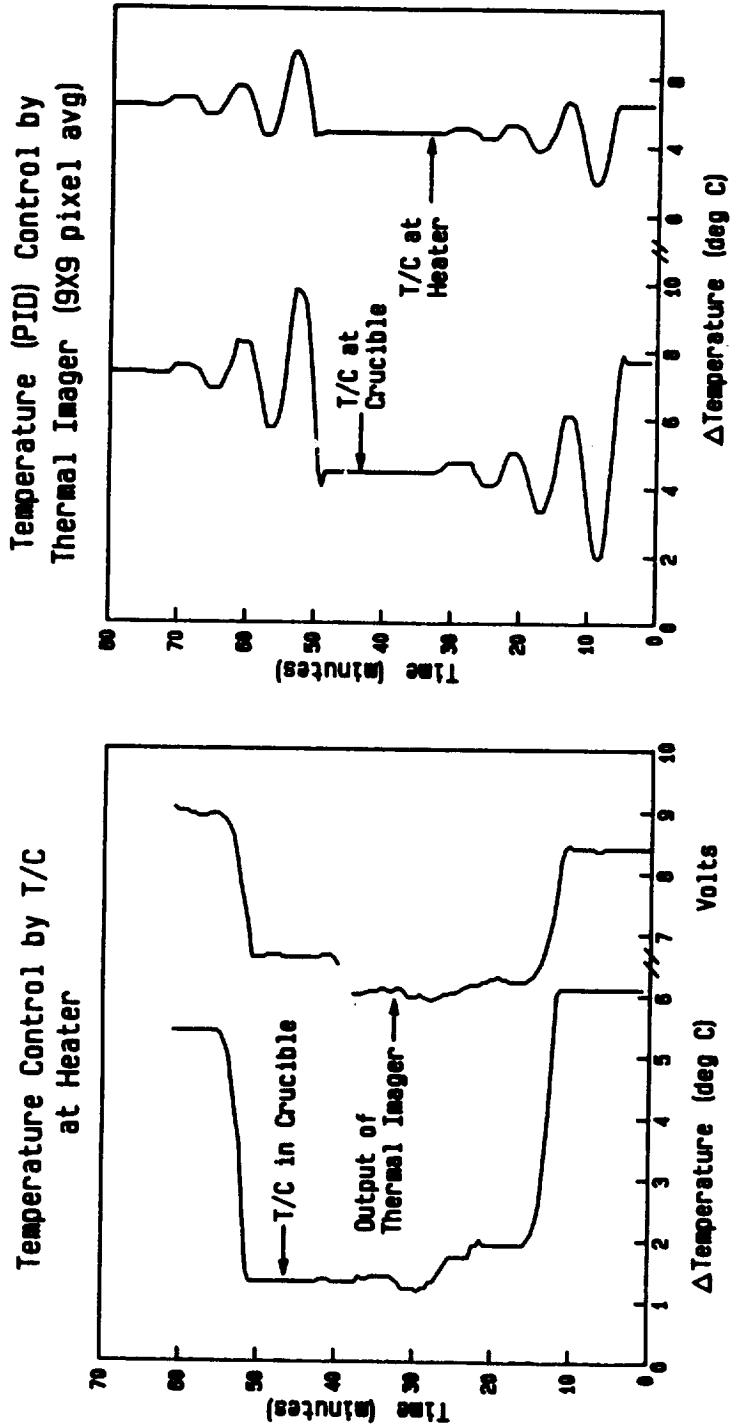
Temperature Control by T/C at Heater

Figure 12

Calibration of the thermal imager. The plot on the left is the output of a thermocouple located in the crucible. The plot on the right depicts the output of the thermal imager scaled to permit plotting on the same instrument. Results are the same as for the technique illustrated in figure 11. See text.

404